Biophysical *Journal*
Article

Biophysical Society

Oblique circle method for measuring the curvature and twist of mitotic spindle microtubule bundles

Arian Ivec,[1,*] Monika Trupinić,[2] Iva M. Tolić,[2] and Nenad Pavin[1,*]
[1]Department of Physics, Faculty of Science, University of Zagreb and [2]Division of Molecular Biology, Ruđer Bošković Institute, Zagreb, Croatia

ABSTRACT The highly ordered spatial organization of microtubule bundles in the mitotic spindle is crucial for its proper functioning. The recent discovery of twisted shapes of microtubule bundles and spindle chirality suggests that the bundles extend along curved paths in three dimensions, rather than being confined to a plane. This, in turn, implies that rotational forces, i.e., torques, exist in the spindle in addition to the widely studied linear forces. However, studies of spindle architecture and forces are impeded by a lack of a robust method for the geometric quantification of microtubule bundles in the spindle. In this work, we describe a simple method for measuring and evaluating the shapes of microtubule bundles by characterizing them in terms of their curvature and twist. By using confocal microscopy, we obtain three-dimensional images of spindles, which allows us to trace the entire microtubule bundle. For each traced bundle, we first fit a plane and then fit a circle lying in that plane. With this robust method, we extract the curvature and twist, which represent the geometric information characteristic for each bundle. As the bundle shapes reflect the forces within them, this method is valuable for the understanding of forces that act on chromosomes during mitosis.

SIGNIFICANCE During cell division, the mitotic spindle divides the genetic material of the mother cell into two equal parts. Precisely regulated forces within the spindle are required for the proper movement of chromosomes and the functional spindle shape. The focus of most research in the field is on tension forces acting on kinetochores, whereas forces that regulate spatial organization of the whole spindle remain poorly understood. The recent discovery of twisted shapes of microtubule bundles suggests that the bundles extend along curved paths in three dimensions, meaning that rotational forces, in addition to linear forces, exist in the spindle. We develop a robust method to measure the curvature and twist of microtubule bundles, which represent information characteristic for each bundle.

INTRODUCTION

Equal division of the genetic material into two newly formed daughter cells is performed by the mitotic spindle, a complex microstructure that consists of two poles, microtubule bundles extending between the poles, and a large number of associated proteins (1–3). The spindle is a mechanical assembly that generates and regulates the forces required for the segregation of chromosomes. The mechanical properties of the spindle arise from the mechanical properties of its basic building blocks, the microtubule bundles. Microtubules are thin elastic filaments that generate and balance the forces acting on chromosomes, which arise from the activity of motor proteins, as well as from polymerization and depolymerization of the microtubule bundles (4).

It is feasible to directly measure the forces exerted on microtubule bundles (5); however, it is rather challenging because of the small scales involved. To complement such experiments, it is possible to measure the forces indirectly by inferring them from the shape of the microtubule bundle (6–8). This approach is based on the fact that microtubules are inherently straight but can obtain different shapes depending on the forces acting upon them. This approach was used to quantify the bending rigidity of single microtubules (8) and microtubule polymerization forces (7). Similarly, methods to characterize the shape of cytoskeletal filaments such as actin and microtubule bundles, together with the relevant forces, have been developed based on open active contours (9–11) or calculating the Frenet frame (12).

An approach for the quantification of forces based on shapes can also be used on microtubule bundles in the spindle.

Submitted March 1, 2021, and accepted for publication July 27, 2021.

*Correspondence: ivec@phy.hr or npavin@phy.hr

Editor: Dimitrios Vavylonis.

https://doi.org/10.1016/j.bpj.2021.07.024

The shapes of individual microtubule bundles give the entire spindle its characteristic shape, such as mitotic spindles in human cells. Similar spindle shapes can be found in most metazoans (13). Interestingly, even in spindles without centrosomes, e.g., in some protozoan organisms such as amoebas, a similar spindle shape is present (14). The same is the case for plant spindles (15). In some lower eukaryotes, e.g., yeasts, this type of spindle shape is absent because their spindles consist of a single straight microtubule bundle (16). Given that the spindle shape reflects the forces within it, accurate measurement and characterization of the shapes of microtubule bundles are highly important for the understanding of forces that act on chromosomes during mitosis.

We have recently shown that the spindle in human cells is a chiral object, as bundles follow a left-handed helical path (17,18). Chirality is also present in the spindles of amoeba *Naegleria gruberi*, though the twist is right-handed (19). The chirality of the spindle is best visualized by looking at the spindle end on, i.e., along the pole-to-pole axis, to observe the three-dimensional shapes with a helical twist (Fig. 1). This view allows for visualization of microtubule bundles as flower petals. By following the bundles in the direction toward the observer, the petals rotate clockwise if the bundles follow a left-handed helical path, which corresponds to negative values of twist (Fig. 1, end-on view). Vice versa, the petals rotate counterclockwise and have a positive value of twist if the bundles follow a right-handed helical path. The reason for this chirality may be the action of the motor proteins that exert rotational forces on the microtubules, such as kinesin-5 (Kif11/Eg5) (20), whose inhibition leads to the abolishment of left-handed twist (17).

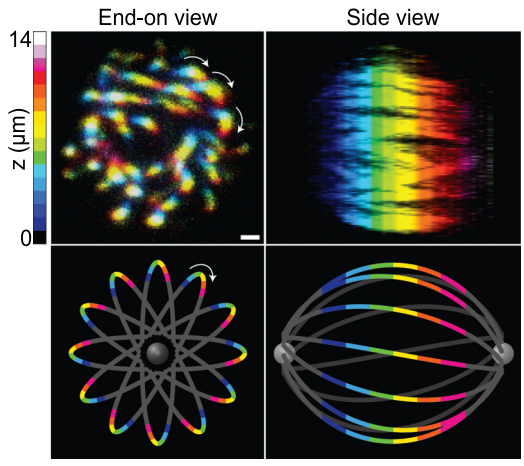

FIGURE 1 End-on view and side view of a human mitotic spindle. (*Top*) Projections of confocal images, color coded for the position along the pole-to-pole axis (see *color bar*), of the metaphase spindle in a live HeLa cell expressing PRC1-GFP shown in the end-on view (*left*) and side view (*right*). Scale bars, 1 μm. (*Bottom*) Schematic representations of spindle microtubule bundles shown in the end-on view (*left*) and side view (*right*). The arrows show the direction of the bundle twist along the pole-to-pole axis when looking toward the observer. The clockwise direction of the arrows indicates left-handed twist. To see this figure in color, go online.

Motor proteins generate these forces by "walking" along a microtubule and performing side steps while switching protofilaments along the same microtubule (21–23).

In this work, we develop a method for the analysis and measurement of the geometrical properties of microtubule bundles within the spindle. To extract information about the shape of a microtubule bundle from experimental data containing a small number of points per bundle, we introduce a robust approach, in which we consider the bundle as a part of a circular arc, leading to two parameters characterizing the bundle. This description allows us to faithfully represent the microtubule bundle and extract the relevant geometrical information, i.e., the curvature and the twist, but it is also simple enough to be done systematically on a wide variety of microtubule bundles.

MATERIALS AND METHODS

Cell lines and microtubule visualization

Twist can be measured in every cell line that has labeled microtubule bundles. This label can be a fluorescent protein tag on a microtubule bundle (e.g., on tubulin) or on proteins that are associated with microtubule bundles in a way that they cover most of the length of the bundle (e.g., PRC1, see Fig. 1). Tags can be inserted into the cells on a plasmid by transfection or endogenously expressed after CRISPR/Cas-9 manipulation. The chosen tags should also allow for the visualization of the spindle poles. It is possible to measure twist both in live and fixed cells. In fixed cells, it is important to perform an appropriate fixation method. Fixation with methanol can often cause spindles to shrink along the z direction, yielding measurements that are not relevant for live cells; thus, care should be taken that the shapes of spindles in fixed cells closely resemble spindles in live cells. In fixed cells, fluorescently labeled antibodies can also be used for tubulin visualization. The spindle in Fig. 1 was imaged as described in Trupinić et al. (18). Further examples of imaging both live and fixed cells for purpose of measuring twist can be found in Novak et al. (17).

Confocal microscopy

To measure twist, whether in live or fixed cells, imaging of the entire spindle needs to be performed. This means that the imaged z-stack needs to be big enough to encompass the spindle from the bottom of the dish to the top of the spindle. Spindles that are oriented horizontally (spindle pole-to-pole axis is parallel with the imaging plane) or vertically (spindle pole-to-pole axis is perpendicular to the imaging plane) are the most appropriate for the analysis. Also, it is important to note the direction of the imaging. It is convenient to image starting from the coverslip and moving upwards because the coverslip is usually easy to determine because of the surrounding cells in interphase that are attached there. The direction of the imaging is important for determining handedness of the twist (right- or left-handed twist). Examples of microscope settings for the purpose of imaging spindles for measuring twist can be found in Novak et al. (17) and Trupinić et al. (18).

RESULTS

Image analysis and data tracking

Individual microtubule bundles need to be tracked to acquire their x, y, and z coordinates in each z plane of the entire z-stack. Examples of such microtubule tracking can be

found in (17). Each spindle has two poles positioned along the pole-to-pole axis, along with N microtubule bundles denoted by index $i = 1, \ldots, N$. The i-th bundle is represented by set of n_i tracked points $\mathbf{T}_{ij} = (x_j, y_j, z_j)_i$ where $j = 1, \ldots, n_i$ is the index of individual points (Fig. 2 *A*). Each bundle is tracked through all z planes in the direction from left centrosome toward the right centrosome (the left centrosome represents the bottom z plane, and the right centrosome represents the highest tracked z plane in the stack). The positions of the centrosomes are the starting and end points of the spindle, so we include this information by extending the coordinates of each single bundle with the centrosome coordinates, with the left centrosome as the starting data point, $\mathbf{T}_{i0}$, and the right centrosome as the ending data point, $\mathbf{T}_{in_i+1}$ (sample data for the spindle from Fig. 1 are given in Table S1), and thus, coordinates of the i-th bundle are indexed $j = 0, \ldots, n_i + 1$. The z plane refers to the imaging plane, which we convert to its corresponding z-coordinate by multiplying with the distance between successive planes set during image acquisition and by a factor of 0.81 to correct for the refractive index mismatch (17). In the example case in Fig. 1, the distance between z planes is equal to 405 nm after correction, and other details of sample preparation are provided in the Materials and methods.

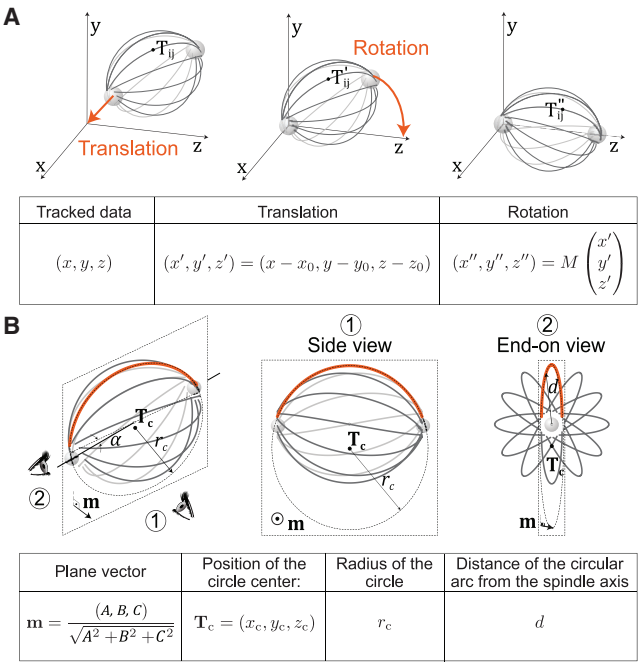

FIGURE 2 Overview of method. (*A*) The spindle, along with the centrosomes and the marked traced bundle point T_{ij}, is positioned at an arbitrary angle and distance from the origin of the coordinate system (*left*). The spindle is translated so that the left centrosome is located at the origin of the coordinate system (*middle*). The spindle is rotated so that the pole-to-pole axis, along with the right centrosome, aligns with the z axis of the coordinate system (*right*). (*B*) A view of the spindle from an arbitrary angle (*left*) where the eyes show the viewing angle for the side view (*1*) and the end-on view (*2*), which are shown in the middle and on the right, respectively. A microtubule bundle (*orange curved line*) is fitted by a circle of radius r_c. The angle between the central spindle axis (*solid line*) and the plane in which the fitted circle lies (*dashed parallelogram*) is denoted. The parameters used to calculate the twist and curvature are named at the bottom of the scheme. To see this figure in color, go online.

Choosing a coordinate system

During imaging, spindles have an arbitrary location and orientation with respect to the laboratory coordinate system. To make tracks of microtubule bundles suitable for analysis, we transform the laboratory coordinate system so that the left centrosome is positioned at the origin of the new coordinate system and the right centrosome is positioned on the z axis (Fig. 2 *A*), which we term the spindle coordinate system. The spindle coordinate system is obtained by two transformations: 1) translation $\mathbf{T}'_{ij} = \mathbf{T}_{ij} - \mathbf{T}_0$, where $\mathbf{T}'_{ij}$ is the transformed coordinate and $\mathbf{T}_0$ is position of the left centrosome (T_0 is given by the *first row* of Table S1), and 2) subsequent rotation $\mathbf{T}''_{ij} = M\mathbf{T}'_{ij}$, where $\mathbf{T}''_{ij}$ are coordinates in the spindle coordinate system and M is the rotation matrix that aligns the pole-to-pole axis with the z axis of the spindle coordinate system and the unit vector $\widehat{\mathbf{z}} = (0, 0, 1)$. The rotation matrix is a textbook problem, and it can be calculated, e.g., as the Rodrigues rotation (24) matrix. A Python implementation is provided in Data S1. Finally, it is convenient to parameterize points by using cylindrical coordinates, $\mathbf{T}''_{ij} = (d_j\cos\phi_j, d_j\sin\phi_j, z_j)_i$, where d_j, ϕ_j, and z_j are, respectively, the radius, azimuth, and axial position.

Fitting a circular arc to the microtubule bundle shapes

To characterize complex three-dimensional shapes of microtubule bundles from noisy experimental data requires a robust approach. In our method, curvature and twist, which measure the extent the bundles extend along curved paths in three dimensions, are the geometrical quantities that represent the information about the bundle shapes. To obtain these quantities from the experimental traces, we fit a circular arc extending through three dimensions to these data.

To fit a circular arc in an easily reproducible way, we first fit a plane, and then fit a circle that lies in this plane (Fig. 2 *B*). In the rest of this section, we focus on one microtubule bundle only, thus we omit the bundle index i.

In the first step, we fit the best-fitting least-squares distance plane $Ax + By + Cz + D = 0$, where A, B, C, and D are the parameters of the general form equation of the plane, which we term the bundle plane, to the traced data. We solve the total least-squares problem by using the singular value decomposition method (25). The normal unit vector of the bundle plane is given by $\mathbf{m} = (A, B, C)/\sqrt{A^2 + B^2 + C^2}$. We denote the angle of vector $\mathbf{m}$ with respect to the pole-to-pole axis as α, which we calculate from the scalar product $\cos\alpha = \mathbf{m} \cdot \widehat{\mathbf{z}}$.

In the second step, we fit a circle to the data by choosing only from those circles that lie in the bundle plane. We calculate the projection of the traced bundle points onto the bundle plane and fit a circular arc to them. Here, we use the HyperLS algorithm (26) because fitting a circle with standard methods (27) is not suitable for straight bundles. The fitting parameters are the radius of the circle, r_c, and the position of the circle center, $\mathbf{T}_c = (x_c, y_c, z_c)$. These parameters, together with the normal vector of the bundle plane, determine the geometry of our traced bundle.

Calculation of the curvature and twist from the fitting parameters

Based on the fitting parameters, we can infer the curvature and twist of the microtubule bundle. The curvature of the bundle can be directly calculated from the radius of the fitted circle,

$$\kappa = \frac{1}{r_c}. \tag{1}$$

The twist, however, cannot be calculated in a straightforward manner. We introduce the twist value, ω, as a change of the azimuthal angle with respect to the axial position

$$\omega = \frac{\mathrm{d}\phi}{\mathrm{d}z}. \tag{2}$$

Please note that this value corresponds to the reciprocal value of the helical pitch multiplied by 2π. The right-hand side of Eq. 2 can be calculated from the slope of the microtubule bundle with respect to the pole-to-pole axis as $\tan(\pi/2 - \alpha) = d \times (\mathrm{d}\phi/\mathrm{d}z)$, where we utilized the fact that the bundle plane vector $\mathbf{m}$, which defines the angle α, is perpendicular to the tangent of the microtubule bundle. Here, d corresponds to the radial coordinate in the spindle coordinate system (see Fig. 2 *B*, end-on view). For our case of discrete tracked bundle data points, we average the radius over all traced points $\langle d \rangle = \frac{1}{n_i}\sum_{j=1}^{n_i} d_j$, and thus, Eq. 2 can be written as

$$\omega = f\frac{\cot\alpha}{\langle d \rangle}, \tag{3}$$

where f is a dimensionless corrective factor, which we introduce to consider the approximative approach of the method because of fitting a circular arc to the bundle segment. The corrective factor depends on the geometry of the bundle, but for bundle segments significantly shorter than the spindle length one can use $f = 1$, as shown in the Error analysis. A Python implementation is provided in Data S2.

Detailed worked example: synthetic spindle

To demonstrate the workings of our method, we provide a detailed worked example on a made-up mitotic spindle in a spindle coordinate system, which mimics the one shown in the schematic in Fig. 2 *B* but also includes noise to make it closer to experimental data. We construct a synthetic spindle as a series of mathematically defined curves, which are evenly distributed around the z axis. Furthermore, to mimic discrete imaging planes, we choose to assign to the z coordinates discrete values of $z_j = L_0 + j\Delta L$, where $j = 1, \ldots, n$. Here, $L_0 + \Delta L$ and $L_0 + n\Delta L$ denote the starting point and ending z coordinates of the synthetic bundle segments. Because all bundles are composed of the same number of points, parameter n has the same value for all bundles. To do this, we first define a bundle as a twisted circular arc:

$$\mathbf{B}(z_j) \equiv \begin{bmatrix} \cos(\omega_0 z_j) & \sin(\omega_0 z_j) & 0 \\ -\sin(\omega_0 z_j) & \cos(\omega_0 z_j) & 0 \\ 0 & 0 & 1 \end{bmatrix} \times \begin{pmatrix} \sigma\eta_x(z_j) \\ \sqrt{R_0^2 - (z_j - L/2)^2} + y_0 + \sigma\eta_y(z_j) \\ z_j \end{pmatrix}. \tag{4}$$

The first term is a matrix that twists the bundle by twist parameter ω_0 around the z axis. The second term is a vector that defines the bundle as a circular arc with added noise, where $R_0 = 1/\kappa_0$ is radius of the circular arc, κ_0 is the corresponding curvature, L is the pole-to-pole length of the spindle, and constant $y_0 = -\sqrt{R_0^2 - (L/2)^2}$ is chosen so that that the circular arc extends from one pole to the other. The two independent components of noise, $\eta_x(z_j)$ and $\eta_y(z_j)$, are unit Gaussian white noises, and σ is the intensity of the noise.

To obtain a spindle, we evenly arrange the N bundles around the pole-to-pole axis so that the i-th bundle, $\mathbf{T}_i$, is given by

$$\mathbf{T}_i(z_j) \equiv \begin{bmatrix} \cos\left(\frac{2\pi i}{N}\right) & \sin\left(\frac{2\pi i}{N}\right) & 0 \\ -\sin\left(\frac{2\pi i}{N}\right) & \cos\left(\frac{2\pi i}{N}\right) & 0 \\ 0 & 0 & 1 \end{bmatrix} \mathbf{B}(z_j). \tag{5}$$

The first term represents a matrix that rotates the i-th bundle to obtain a spatial configuration of bundles distributed around the z axis.

Finally, positions of spindle poles are given by

$$\mathbf{T}_{i,0} = \begin{pmatrix} 0 \\ 0 \\ 0 \end{pmatrix}, \quad \mathbf{T}_{i,n+1} = \begin{pmatrix} 0 \\ 0 \\ L \end{pmatrix}. \tag{6}$$

Our method will determine the defined twist of this curve ω, as well as its curvature κ.

Fitting circular arcs to the bundles of the synthetic spindle

We fit a circular arc to the synthetic bundles by using the approach described in the Fitting a circular arc to the microtubule bundle shapes. In the first step, we obtain parameters of the bundle plane, A, B, C, and D. In the second step, we fit the circular arc that lies in the bundle plane and the corresponding radius r_c.

To test our method, we apply the method to four different synthetic spindles shown in Fig. 3. The first and second spindles have short bundle segments with and without noise, whereas the third and fourth spindles have long bundle segments, also with and without noise. In the case with short bundle segments, the twist and curvature obtained from the method closely matches the parameters that define the synthetic spindle, both with and without noise (Fig. 3, *A and B*). This agreement is expected because the fitting curve closely follows the synthetic bundle segments in the case without noise. In the case with long bundle segments, the obtained twist is slightly smaller than the defined one, and the difference between the fitted curve and the synthetic bundle segments becomes visible (Fig. 3, *C and D*).

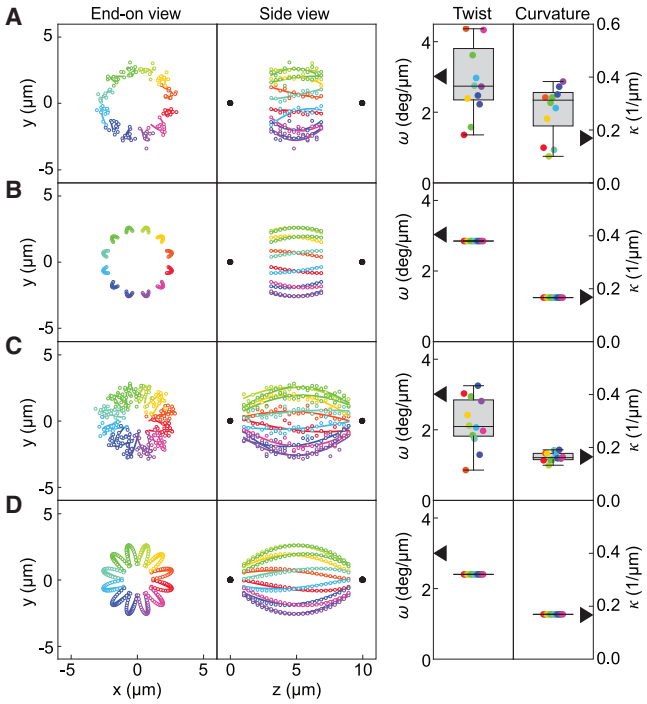

FIGURE 3 Application of method to four synthetic spindles. Synthetic spindles (*colored circles*) are shown together with poles (*black points*), fits to them (*colored lines*) in the side view (*left*) and in the end-on view (*middle*), and corresponding values of twist and curvature (*right*). The first two spindles have short bundle segments, in which 40% of central bundles were calculated, both with noise (A) and without noise (B). The last two spindles have long bundle segments, in which 80% of central bundles were calculated, with noise (C) and without noise (D). Short segments are composed of $n = 12$ points, with noise $\sigma = 0.25$ μm in (A) and $\sigma = 0$ μm in (B). Long segments are composed of $n = 24$ points, with noise $\sigma = 0.25$ μm in (C) and $\sigma = 0$ μm in (D). For all spindles, the values of the other parameters are $\Delta L = 0.33$ μm, $\omega_0 = 3°/\mu$m, $L = 10$ μm, and $R_0 = 6$ μm, which corresponds to the curvature of $\kappa_0 = 0.188$ μm^{-1}. Twist and curvature are shown with individual points and box and whisker plots (median and interquartile range, whiskers extending to 1.5 of the interquartile range). Black arrowheads show the values of parameters ω_0 and κ_0. To see this figure in color, go online.

Error analysis

Because in the case of long bundle segments, the twist we obtain from our method underestimates the value of the twist parameter (Fig. 3, *C and D*), we explored how the discrepancy changes with the length of the bundle segment, normalized by the length of the spindle $\ell = n\Delta L/L$, for noise intensity set to zero, $\sigma = 0$ μm. We determine the twist of synthetic spindles by our method for segment lengths ranging from 0.2 to 10 μm and plot the value of the twist ω obtained from our method divided by the twist parameter, as shown in Fig. 4, *A and B*. The other parameters have a smaller influence on the method. In particular, varying the value of ω_0 from 0 to 9°/μm (Fig. 4 *A*) and R_0/L from 0.6 to 4 (Fig. 4 *B*), we find that the difference in the twist ratios

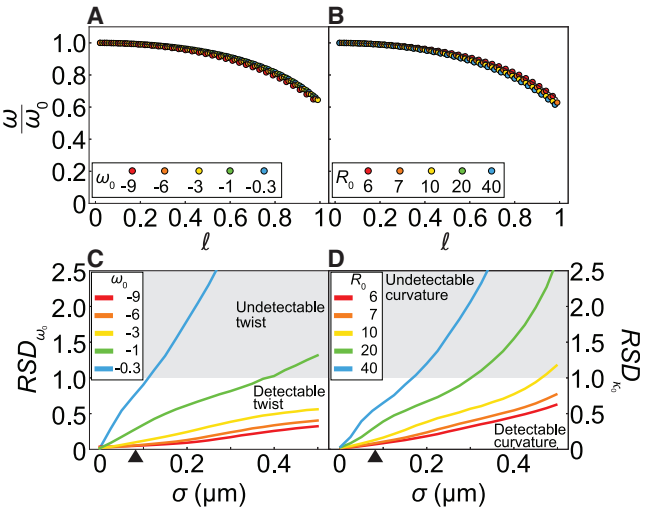

FIGURE 4 Error analysis for twist and curvature of synthetic spindles. (*A*) The dots show the dependence of the twist ratio for a spindle with $\omega_0 = 3°/\mu$m and five different values of R_0, shown in the legend, as a function of the normalized bundle segment length. The values for $R_0 = 20$ μm are not visible because they overlap with values for $R_0 = 40$ μm. (*B*) The dots show the dependence of the twist ratio for a spindle with $R_0 = 6$ μm and five different values of ω_0, shown in the legend, as a function of the normalized bundle segment length. In both (*A*) and (*B*), the thick black line shows the function $f(\ell)$ from Eq. 7 and there is no noise, $\sigma = 0$ μm. (*C*) The lines show the relative dispersion of the curvature, for a spindle with $\omega_0 = 3°/\mu$m and five different values of R_0, shown in the legend, as a function of the noise intensity. (*D*) The lines show the relative dispersion of the method for twist, for a spindle with $R_0 = 6$ μm and five different values of ω_0, shown in the legend, as a function of the noise intensity. In both (*C*) and (*D*), $\ell = 0.6$, the undetectable region is shaded gray, and black arrowheads denote $\sigma = 0.08$ μm. In all panels, $L = 10$ μm, $N = 20{,}000$, and $n = 18$. To see this figure in color, go online.

for different values of R_0 does not exceed 5% and that the difference in the twist ratio for different values of ω_0 does not exceed 4.5%. In real spindles, the twist of bundle ranges from 0 to 20°/μm and the width/length ratio R/L from 0.6 to 0.8 (18), making it possible to treat the error solely as a function of the bundle segment length ℓ.

The value of the twist obtained by our method systematically underestimates the exact value for longer bundle segments, which we can use to remedy this discrepancy. To obtain, by our method, a value of the twist close to the actual value, we need to calculate the corrective factor f in Eq. 3. Approximatively, this function is given by

$$f(\ell) = 1 - 0.178\,\ell^2 - 0.178\,\ell^4. \quad (7)$$

Because the synthetic spindle is similar to spindles found in HeLa cells, this phenomenological function can be used for all bundles in HeLa spindles and also for spindles that have shapes similar to HeLa cells. For the majority of bundles, this correction will be less than 5% (18,19).

To explore whether we can use our method to detect twist and curvature in noisy experimental data, we apply our method to the synthetic spindle and estimate for which noise intensity values twist and curvature are detectable. Here, we calculate the relative dispersion of a measured twist as $RSD_{\omega_0} = \frac{1}{\omega_0}\sqrt{\frac{1}{N}\sum_{i=1}^{N}(\omega_i - \omega_0)^2}$ for different values of the noise intensity and twist (Fig. 4 *C*). We found that for a broad range of noise intensity values around 80 nm, which is equivalent to the pixel size of the confocal microscope, and twist values around 3°/μm, the relative dispersion was significantly below 1. A value of RSD below 1 signifies that the twist is detectable, i.e., $RSD = 1$ is the detection limit. Similarly, we calculate the relative dispersion of the curvature as $RSD_{\kappa_0} = R_0\sqrt{\frac{1}{N}\sum_{i=1}^{N}(1/R_i - 1/R_0)^2}$. We have found that for a broad range of values typical for spindles, the curvature was detectable (Fig. 4 *D*). Based on these results, we conclude that the method can reliably detect twist and curvature in noisy experimental data.

Application of the oblique circle method to real spindles

To apply our method to real spindles and compare the results with the method from (17), we first analyzed the HeLa cell spindle from Fig. 1 (Table S2) and obtained fits and values for the curvature and twist (Fig. 5; Table S3). The resulting twist is $\omega = -2.3 \pm 0.3$°/μm (mean $\pm$ standard error), and the curvature is $\kappa = 0.08 \pm 0.01$°/μm. The value of twist is consistent with the value of obtained by using the method from Novak et al. (17), $\omega = -2.3 \pm 0.4$°/μm. The value of curvature is similar to the value obtained from the program SOAX (10), which is based on stretching open active contours, $\kappa = 0.07 \pm 0.01$°/μm, with SOAX parameters chosen in such a way that number of converged snakes is similar to the number of tracked bundles (Data S3).

Furthermore, to explore how the oblique circle method performs on a wide range of test cases, we applied it to spindles from the HeLa cell line, including live and fixed cells stained with different methods and with applied STLC (S-trityl-L-cysteine) and Lat A (Latrunculin A) treatments, from Novak et al. (17). The obtained results are similar to those from Novak et al. (17), even though the obtained values were slightly lower (Fig. 6).

DISCUSSION

Curvature and twist provide geometrical information about the shape of the bundle. Based on these geometrical parameters, we can infer information about rotational forces, i.e., bending and twisting moments. Curvature can provide an estimate of the bending moment acting upon the bundle $M_{\text{bend}} = EI/r_c$, where r_c is the radius of curvature measured for a microtubule bundle and EI is its flexural rigidity given as Young's modulus times the second moment of inertia of the cross section. In the case of bundles with multiple microtubules, the flexural rigidity depends on the number of microtubules in microtubule bundles and how tightly they are linked (28). From fluorescence analysis, the number of microtubules in bundles was estimated to be between 14 and 21 k-fibers (29,30).

Twist characterizes to what extent bundles rotate around the spindle pole-to-pole axis. Intuitively, one can expect

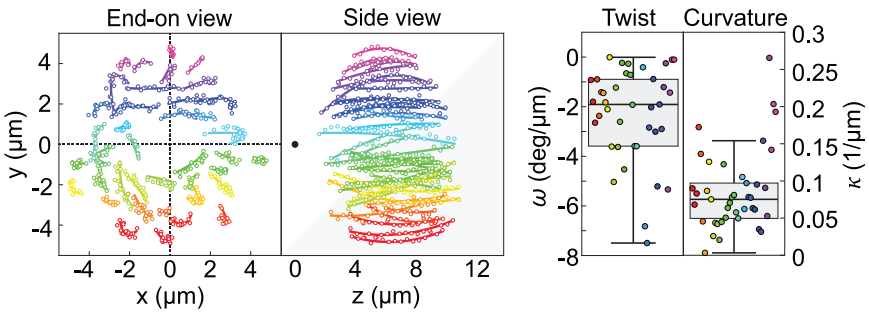

FIGURE 5 Application of the oblique circle method to the HeLa cell mitotic spindle from Fig. 1. Tracked microtubule bundles are shown in the end-on view (*left*) and side view (*right*). Each bundle is represented by a different color, thin circles mark the manually traced points along the bundle, and thick lines show circular arcs of the fitted circles. The spindle poles are represented as black dots in the side view. Box and whisker plots (median and interquartile range, whiskers extending to 1.5 of the interquartile range) of the twist and curvature of each bundle are given. This HeLa cell spindle shows a strong left-handed twist. To see this figure in color, go online.

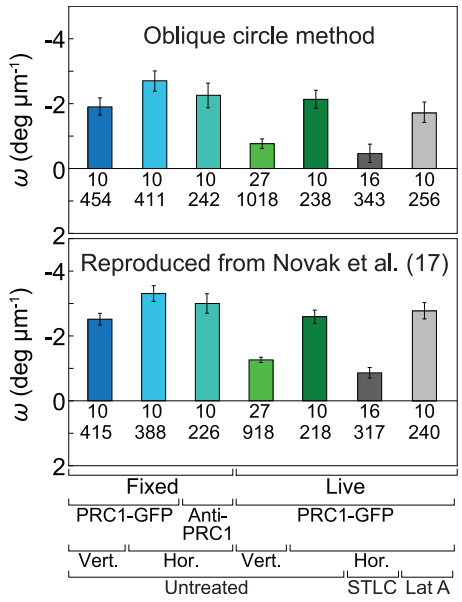

FIGURE 6 Calculation of the twist of spindles in HeLa cells from Novak et al. (17). The average twist of spindles in different conditions, including vertical and horizontal spindles, fixed and live cells, untreated and treated cells, is analyzed with the oblique circle method (*top*) and reproduced from Novak et al. (17) (*bottom*). Error bars, mean ± standard error. Cell lines were HeLa cells expressing PRC1-GFP (*first*, *second*, *fourth*, *fifth*, *sixth*, and *seventh bars*) and unlabeled HeLa cells immunostained for PRC1 (*third bar*). Numbers below the bars represent the number of cells (*top*) and bundles (*bottom*). Note that the number of bundles is larger for twist measured by the oblique circle method because the method includes all bundles. Bottom graph was reproduced with permission from Novak et al. (17), from Figs. 1 and 2. To see this figure in color, go online.

that twist is related to twisting moment within these bundles. This is indeed the case for spindles described by the model from (17), in which microtubule bundles that are intrinsically straight extend radially from spindle poles. In this case, we can obtain an estimate for the twisting moment acting upon the microtubule bundle $M_{\text{twist}} = \omega\tau$, where ω is the measured twist and τ is the torsional rigidity of the microtubule bundle (17,31).

In the study of Novak et al. (17), twist was calculated for short bundles, calculating twist for finite segments Δz using only the starting and ending points of the bundle, whereas we excluded bundle data points close to the poles and entire bundles close to the pole-to-pole axis. With the oblique circle method, we calculated ω by utilizing all data points, including those with longer bundle segments and bundles closer to the pole-to-pole axis. By doing this, we replicated all key findings, though the obtained twist was slightly lower. The oblique circle method has the advantage of being more robust and applicable to a greater variety of microtubule bundles.

Fitting the simple shape of a circular arc is a straightforward approach to extract the most important geometrical parameters from the data obtained from confocal microscopy, namely from microtubule bundles that have a low number of data points and make less than one helical turn. The oblique circle method cannot be applied to microtubule bundles that make several helical turns because such shapes cannot be approximated by a circular arc. The usual techniques of signal processing are designed for working with microtubule bundles that make several helical turns (32,33), but for the same reason, they are less suitable for fitting microtubule bundles in spindles.

Our method could also be applied to the data of bundle shapes obtained from super-resolution or electron microscopy and provides more accurate information about the curvature and twist of microtubule bundles. High-resolution microscopy data might also allow for the use of more complex fitting techniques (9–12), making it possible to obtain not only the twist and curvature but also other geometric parameters. Further comparison of different fitting methods would be necessary to identify an optimal approach for spindle microtubule bundle characterization.

The discovery that microtubule bundles in the mitotic spindle are twisted in a helical manner opens an exciting area of research on the potential biological roles of spindle chirality and the mechanisms generating this curious type of asymmetry, which is why we developed a method to measure the twist and the curvature of microtubule bundles to characterize the shape of the spindle. The method allows for easy extraction of information about the relevant aspects of microtubule bundle geometry. By utilizing the characteristic shape of microtubule bundles in the spindle, it is possible to characterize them in a reproducible manner. This approach opens up new lines of studies, allowing for efficient mapping of the similarities and differences between shapes of spindles in various cell types and organisms. Because the spindle shapes reflect the forces within them, this method will be instrumental for the understanding of forces that act on chromosomes during cell division.

SUPPORTING MATERIAL

Supporting material can be found online at https://doi.org/10.1016/j.bpj.2021.07.024.

AUTHOR CONTRIBUTIONS

A.I. developed the method for twist and curvature measurement. M.T. analyzed the experimental data in Fig. 1. A.I. measured the twist from bundle traces. A.I., N.P., and M.T. wrote the manuscript, with input from I.M.T. A.I. assembled the figures. N.P. and I.M.T. conceived and supervised the project.

ACKNOWLEDGMENTS

The authors thank Ina Poser and Tony Hyman (Max Planck Institute of Molecular Cell Biology and Genetics, Dresden, Germany) for HeLa-Kyoto BAC cell line stably expressing PRC1-GFP, Barbara Kokanović for the image of HeLa PRC1-GFP spindle used in Fig. 1, all members of the Pavin and Tolić groups for helpful discussions, and Ivana Šarić for the drawings.

Research in the Pavin and Tolić groups is supported by the European Research Council (Synergy Grant, GA number 855158, granted to I.M.T. and N.P.) and Croatian Science Foundation (projects IP-2019-04-5967 granted to N.P. and PZS-2019-02-7653 granted to I.M.T.; the work of doctoral students A.I. and M.T. have been supported by the corresponding "Young researchers' career development project – training of doctoral students"), the QuantiXLie Center of Excellence, a project co-financed by the Croatian Government and European Union through the European Regional Development Fund—the Competitiveness and Cohesion Operational Programme (grant KK.01.1.1.01.0004). I.M.T. acknowledges earlier support from the European Research Council (Consolidator Grant, GA number 647077).

REFERENCES

1. McIntosh, J. R., M. I. Molodtsov, and F. I. Ataullakhanov. 2012. Biophysics of mitosis. *Q. Rev. Biophys.* 45:147–207.
2. Pavin, N., and I. M. Tolić. 2016. Self-organization and forces in the mitotic spindle. *Annu. Rev. Biophys.* 45:279–298.
3. Prosser, S. L., and L. Pelletier. 2017. Mitotic spindle assembly in animal cells: a fine balancing act. *Nat. Rev. Mol. Cell Biol.* 18:187–201.
4. Howard, J. 2001. Mechanics of Motor Proteins and the Cytoskeleton. Sinauer Associates, Sunderland, MA.
5. Nicklas, R. B. 1983. Measurements of the force produced by the mitotic spindle in anaphase. *J. Cell Biol.* 97:542–548.
6. Pavin, N., and I. M. Tolić. 2021. Mechanobiology of the mitotic spindle. *Dev. Cell.* 56:192–201, Published online November 24, 2020.
7. Dogterom, M., and B. Yurke. 1997. Measurement of the force-velocity relation for growing microtubules. *Science.* 278:856–860.
8. Gittes, F., B. Mickey, …, J. Howard. 1993. Flexural rigidity of microtubules and actin filaments measured from thermal fluctuations in shape. *J. Cell Biol.* 120:923–934.
9. Smith, M. B., H. Li, …, D. Vavylonis. 2010. Segmentation and tracking of cytoskeletal filaments using open active contours. *Cytoskeleton (Hoboken).* 67:693–705.
10. Xu, T., D. Vavylonis, …, X. Huang. 2015. SOAX: a software for quantification of 3D biopolymer networks. *Sci. Rep.* 5:9081.
11. Xu, T., D. Vavylonis, and X. Huang. 2014. 3D actin network centerline extraction with multiple active contours. *Med. Image Anal.* 18:272–284.
12. Jikeli, J. F., L. Alvarez, …, U. B. Kaupp. 2015. Sperm navigation along helical paths in 3D chemoattractant landscapes. *Nat. Commun.* 6:7985.
13. Crowder, M. E., M. Strzelecka, …, R. Heald. 2015. A comparative analysis of spindle morphometrics across metazoans. *Curr. Biol.* 25:1542–1550.
14. Walsh, C. J. 2012. The structure of the mitotic spindle and nucleolus during mitosis in the amebo-flagellate Naegleria. *PLoS One.* 7:e34763.
15. Zhang, H., and R. K. Dawe. 2011. Mechanisms of plant spindle formation. *Chromosome Res.* 19:335–344.
16. McCully, E. K., and C. F. Robinow. 1971. Mitosis in the fission yeast *Schizosaccharomyces pombe*: a comparative study with light and electron microscopy. *J. Cell Sci.* 9:475–507.
17. Novak, M., B. Polak, …, N. Pavin. 2018. The mitotic spindle is chiral due to torques within microtubule bundles. *Nat. Commun.* 9:3571.
18. Trupinić, M., I. Ponjavić, …, I. M. Tolić. 2020. Twist of the mitotic spindle culminates at anaphase onset and depends on microtubule-associated proteins along with external forces. *bioRxiv* https://doi.org/10.1101/2020.12.27.424486.
19. Velle, K. B., M. Trupinić, …, P. Wadsworth. 2021. *Naegleria's* mitotic spindles are built from unique tubulins and highlight core spindle features. *bioRxiv* https://doi.org/10.1101/2021.02.23.432318.
20. Yajima, J., K. Mizutani, and T. Nishizaka. 2008. A torque component present in mitotic kinesin Eg5 revealed by three-dimensional tracking. *Nat. Struct. Mol. Biol.* 15:1119–1121.
21. Ramaiya, A., B. Roy, …, E. Schäffer. 2017. Kinesin rotates unidirectionally and generates torque while walking on microtubules. *Proc. Natl. Acad. Sci. USA.* 114:10894–10899.
22. Can, S., M. A. Dewitt, and A. Yildiz. 2014. Bidirectional helical motility of cytoplasmic dynein around microtubules. *eLife.* 3:e03205.
23. Bormuth, V., B. Nitzsche, …, S. Diez. 2012. The highly processive kinesin-8, Kip3, switches microtubule protofilaments with a bias toward the left. *Biophys. J.* 103:L4–L6.
24. Rodrigues, O. 1840. Des lois geometriques qui regissent les desplacements d'un systeme solide dans l'espace et de la variation des coordonnees provenant de deplacements consideres independamment des causes qui peuvent les produire. *J. Math. Pures Appl.* 5:380–440.
25. Golub, G. H., and C. Reinsch. 1971. Singular value decomposition and least squares solutions. *In* Handbook for Automatic Computation: Volume II: Linear Algebra F. L. Bauer, J. H. Wilkinson, and C. Reinsch, eds.. Springer, pp. 134–151.
26. Kanatani, K., and P. Rangarajan. 2011. Hyper least squares fitting of circles and ellipses. *Comput. Stat. Data Anal.* 55:2197–2208.
27. Taubin, G. 1991. Estimation of planar curves, surfaces, and nonplanar space curves defined by implicit equations with applications to edge and range image segmentation. *IEEE Trans. Pattern Anal. Mach. Intell.* 13:1115–1138.
28. Rubinstein, B., K. Larripa, …, A. Mogilner. 2009. The elasticity of motor-microtubule bundles and shape of the mitotic spindle. *Phys. Biol.* 6:016005.
29. Kajtez, J., A. Solomatina, …, I. M. Tolić. 2016. Overlap microtubules link sister k-fibres and balance the forces on bi-oriented kinetochores. *Nat. Commun.* 7:10298.
30. Dudka, D., A. Noatynska, …, P. Meraldi. 2018. Complete microtubule-kinetochore occupancy favours the segregation of merotelic attachments. *Nat. Commun.* 9:2042.
31. Landau, L. D., E. M. Lifshitz, …, W. H. Reid. 1986. Theory of ElasticityVolume 7. Elsevier Science, Amsterdam.
32. Friedrich, B. 2020. frenet_robust.zip, MATLAB Central File Exchange https://www.mathworks.com/matlabcentral/fileexchange/47885-frenet_robust-zip.
33. Friedrich, B. 2020. powersmooth, MATLAB Central File Exchange https://www.mathworks.com/matlabcentral/fileexchange/48799-powersmooth.